

## Determination of Mean Cluster Sizes by Water Capture

Michel Macler\* and Young K. Bae

Hughes STX/USAF Phillips Laboratory, Propulsion Directorate, OLAC PL/RKS, 10 East Saturn Boulevard  
Edwards AFB, California 93524-7680

Received: July 9, 1996; In Final Form: October 28, 1996<sup>⊗</sup>

Argon clusters ( $\text{Ar}_{30-400}$ ) produced in a supersonic expansion were doped with water using the pickup method and subsequently electron impact ionized. Charged fragments were detected by a triple-quadrupole mass spectrometer. The intensities of the water-containing fragment peaks ( $\text{Ar}_n\text{H}_2\text{O}^+$ ,  $n = 4-7$ ) versus water pressure followed Poisson distributions, from which capture cross sections were derived. These cross sections corresponded to cluster sizes in agreement with published results for our range of stagnation conditions. The measurement of water capture cross sections has been shown to provide a convenient means of determining van der Waals cluster mean sizes.

### Introduction

The measurement of the mean cluster size is very important to the characterization of a cluster beam. Van der Waals cluster beams are typically produced by rapidly expanding a gas through a nozzle, into a vacuum chamber.<sup>1-3</sup>

The earliest technique used to characterize clusters was electron impact ionization/time-of-flight mass spectrometry.<sup>4</sup> Unfortunately, van der Waals clusters are extensively fragmented by the ionization process. The resulting ionized fragments, especially for small clusters, are not at all representative of the parent cluster size.<sup>5</sup> A correction method has been developed to alleviate this problem,<sup>5</sup> but it complicates the data analysis.

Other types of measurements have been carried out that require sophisticated equipment and/or difficult data analysis like electron diffraction<sup>7,8</sup> and collisional scattering<sup>9</sup> or require an absolute calibration like Rayleigh scattering.<sup>10</sup>

In this work we have used what most experimentalists consider an irritating problem, namely, the pickup of background water molecules by clusters, and turned it into a simple, direct, and reliable cluster size measurement technique using the methods of the pioneering works of Gough et al.<sup>11</sup> and Lewerenz et al.<sup>12</sup>

### Experimental Section

For the production of an intense cluster beam, a Campargue source<sup>13</sup> was used. This type of source utilizes a relatively high pressure ( $\sim 0.2$  Torr) in the discharge chamber, yielding conditions favorable to producing clusters efficiently. However, the high gas density achieved over a long path requires very precise skimming to avoid destroying the beam.

Figure 1 displays the apparatus schematically, i.e., not to scale. On the left is the nozzle discharge chamber. The sonic nozzle with a throat diameter  $d$  of 0.17 mm is coupled to a cold head located inside a shroud. This head is cooled by a closed cycle He refrigerator, the temperature of which can be controlled by throttling. The inside of the shroud is sealed off from the discharge chamber with a stainless steel diaphragm. The first skimmer, placed 6 mm from the nozzle exit plane, is attached to the nozzle assembly with four Nylon spacers. It

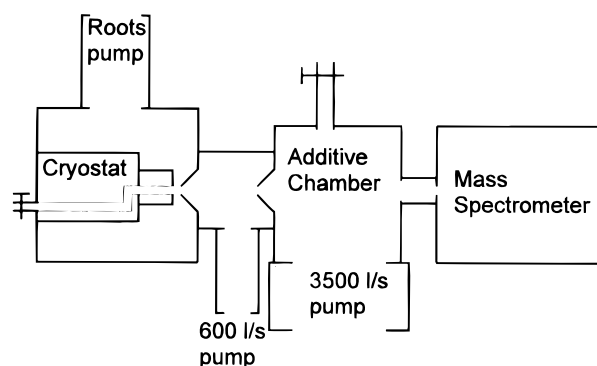


Figure 1. Schematic of the apparatus.

has a 1 mm entrance diameter. The skimmer assembly is also attached to a stainless steel diaphragm. This diaphragm is used to separate the first pumping stage from the second one. The discharge chamber is connected through a gate valve to a Roots blower pump with a pumping speed of  $\approx 200$  L/s. Typical pressure under operating conditions is  $2 \times 10^{-2}$ – $2 \times 10^{-1}$  Torr.

The second pumping stage is pumped out by a turbomolecular pump with a nominal speed of 600 L/s. The second skimmer, or collimator, is attached to a shroud and placed 30 mm from the nozzle exit plane and has a 2 mm diameter entrance aperture. Under operating conditions, this region reaches a pressure of  $10^{-(4-5)}$  Torr.

The third pumping stage is evacuated by a turbomolecular pump of 3500 L/s nominal speed. It is used as the doping chamber, with an effective doping length of  $\sim 100$  cm. The doping pressure is monitored by a Bayard-Alpert type ionization gauge which is calibrated against a capacitance manometer. The typical background pressure of the doping chamber is  $10^{-7}$  Torr and is mostly due to water.

Clusters are detected by electron impact ionization mass spectrometry. Doped clusters pass through a 6 mm diameter aperture and through a chamber pumped by an 8 in. diameter cryopump with a nominal pumping speed of 1200 L/s. The typical pressure in this chamber is  $10^{-6}$  Torr under operation. The cluster beam is chopped by a tuning fork for phase sensitive detection and enters the quadrupole mass spectrometer chamber through a 3 mm diameter aperture. The cluster beam is electron impact ionized with 100 eV electrons from a concentric electron gun. Cluster ions are extracted from the ionization region by a

\* To whom correspondence should be addressed.

<sup>⊗</sup> Abstract published in *Advance ACS Abstracts*, December 15, 1996.

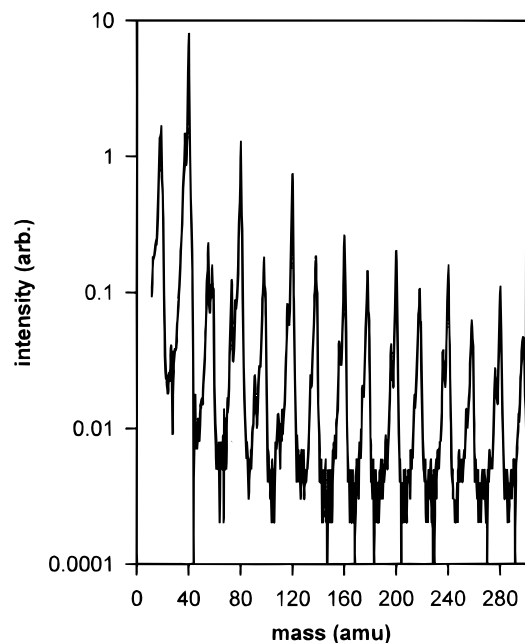


**Figure 2.** Mass spectrum obtained for electron impact ionized water doped Ar clusters. The intensity scale is a common log scale, because it highlights the lower intensity peaks.  $p_0 = 1.15$  atm,  $T_0 = 160$  K, and the water pressure is  $3.47 \times 10^{-6}$  Torr. The mass peaks at  $40n$  correspond to pure Ar fragments. Mass peaks appearing at  $40n + 18$  correspond to  $\text{Ar}_n\text{H}_2\text{O}^+$  fragments. One can see a shoulder on the low mass side of the pure Ar fragments. This shoulder corresponds to  $\text{Ar}_n(\text{H}_2\text{O})_2^+$  fragments, appearing at mass  $40n + 36$ .

set of six electrostatic lenses, mass analyzed by a quadrupole mass spectrometer, and detected by a channeltron multiplier. The quadrupole mass spectrometer chamber is pumped by a 600 L/s turbomolecular pump. Its pressure is typically  $\sim 10^{-7}$  Torr; thus, the effect of collisional fragmentation in the detection chamber on the measured spectra is insignificant.

The analog signal from a preamplifier–amplifier combination connected to the channeltron multiplier is digitized by a 16-bit analog-to-digital converter. The digital signal is stored and analyzed on a personal computer, which is also used to run and control the mass spectrometer via a 16-bit digital-to-analog converter. Typical mass spectra have a 1–2 amu resolution in the 10–300 amu range.

Since the stagnation pressure  $p_0$ , the stagnation temperature  $T_0$ , and the nozzle throat diameter  $d$  determine the flow conditions, they are the parameters that govern the clustering process.<sup>2,3,6</sup> In this work, we used only one nozzle size. Therefore, to produce different mean cluster sizes,  $p_0$  was varied in the 1.15–3.4 atm range and  $T_0$  spanned the 100–300 K range. In the doping chamber, the water pressure was increased progressively from  $10^{-7}$  to  $10^{-4}$  Torr, resulting in an increasing level of Ar cluster doping, up to the formation of pure water clusters.

## Results

Figure 2 shows a typical mass spectrum for water-doped Ar clusters. As expected, the signal originates from cluster fragments. Pure Ar fragments appear at mass  $40n$ , while  $\text{Ar}_n\text{H}_2\text{O}^+$  fragments appear at mass  $40n + 18$ . The relative intensities of the  $\text{Ar}_n\text{H}_2\text{O}^+$  peaks with respect to  $\text{Ar}_n$  peaks depend on the water pressure in the doping chamber.

For a set of given stagnation conditions, mass spectra, such as that presented in Figure 2, were recorded for different doping chamber pressures. The intensities of individual  $\text{Ar}_n\text{H}_2\text{O}^+$  peaks were plotted against the water pressure. Figure 3 shows such

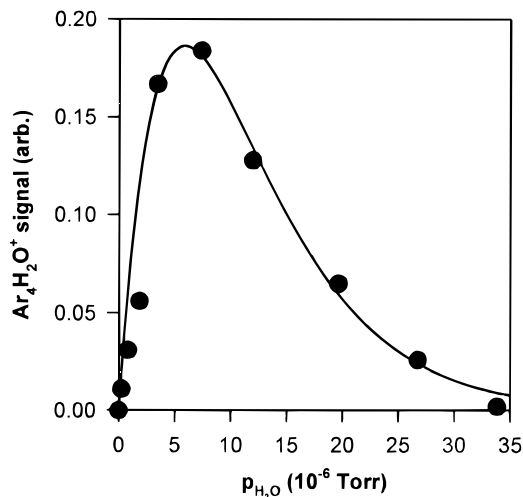


**Figure 3.** Variation of the peak intensity at mass 178, corresponding to the  $\text{Ar}_4\text{H}_2\text{O}^+$  fragment, with water pressure in the pickup chamber.  $p_0 = 1.15$  atm and  $T_0 = 160$  K. The line represents the Poisson fit to the data. The quality of the fit is representative of most recorded data. The calculated mean cluster size is  $N = 87$ .

a plot for the  $\text{Ar}_4\text{H}_2\text{O}^+$  mass peak; it is typical of  $\text{Ar}_n\text{H}_2\text{O}^+$  peaks. The experimental data were fitted to a Poisson distribution,<sup>12</sup> which is expected for random events. Figure 3 represents such a distribution. Since this process and its analysis was discussed at length by Lewerenz et al.,<sup>12</sup> only the details relevant to this work will be outlined. For one water molecule picked up, we have

$$I = K\alpha L \exp(-\alpha L) \quad (1)$$

where  $I$  is the peak intensity,  $K$  is a constant, and  $L$  is the length of the pickup region. The parameter  $\alpha$  is given by

$$\alpha = n\sigma_{\text{capture}}F_{a0}(\infty, x) \quad (2)$$

where  $\sigma$  is the capture cross section,  $n$  is the number density of water, and  $F_{a0}(\infty, x)$  is a velocity-averaging correction factor for an assumed velocity independent hard-sphere potential;  $x$  is the ratio of the cluster beam velocity to the dopant molecule velocity. It should be noted that  $\alpha$  is a linear function of the water number density. Tabulated values of  $F_{a0}(\infty, x)$  are available.<sup>14</sup> For this set of experiments,  $F_{a0}(\infty, x)$  is in the range 1.17–2.1. Equations 1 and 2 were used to calculate capture cross sections. Curve fits of  $I$  versus  $n$  gave  $\alpha$ , and thus  $\sigma$ . It is also possible to determine  $\sigma$  from the position of the maximum of the Poisson distribution, as  $\sigma n_{\text{max}}$  is the inverse of  $F_{a0}(\infty, x) \cdot L$ . Here  $n_{\text{max}}$  is the water number density at the maximum of the distribution.

Experimental data such as that presented in Figure 3 were fitted to eq 1 using a Levenberg–Marquardt algorithm. The resulting cross sections were averaged for masses corresponding to the  $\text{Ar}_{4-7}(\text{H}_2\text{O})^+$  fragments. For these fragments, cross sections were found to be independent of the mass and showed little dispersion. We assumed that the sticking coefficient of water on Ar clusters was unity, based on the strength of the Ar– $\text{H}_2\text{O}$  interaction potential. We also assumed that the clusters were spherical. Capture cross sections were converted into mean cluster sizes using eqs 3 and 4 shown below. First, cluster radii were evaluated using the following expression:

$$R_c = (\sigma/\pi)^{1/2} \quad (3)$$

where  $R_c$  is the cluster radius, and  $\sigma$  is the capture cross section. For an Ar van der Waals radius  $R_{\text{vw}}$  of  $3.6 \times 10^{-8}$  cm, the

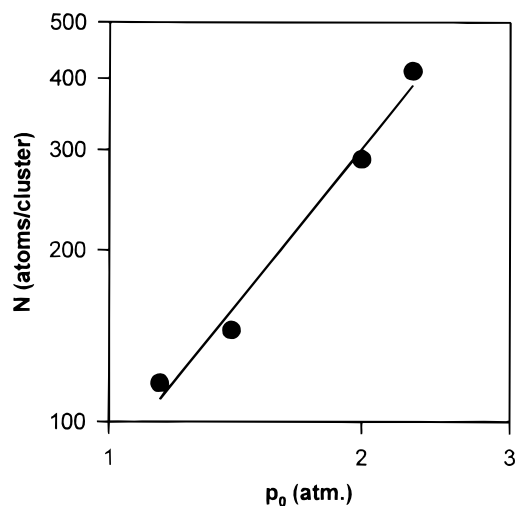


**Figure 4.** Variation in cluster size at 140 K, with a nozzle diameter of 0.17 mm for a range of stagnation pressures. The pressure exponent is 1.8.

cluster size  $N$  was defined as

$$N = (4/3\pi)(R_c/R_{vw})^3 = 9 \times 10^{-2} R_c^3 \quad (4)$$

with  $R_c$  expressed in angstroms. One should note that these equations are valid for hard-sphere type interaction and that such interactions are assumed throughout this work. Interactions between water molecules and argon clusters are subject to dipole induced–dipole interactions. These interactions will increase the effective size of the clusters, and the value of  $N$  calculated using eqs 3 and 4 may be overestimating the actual cluster size.

To test the accuracy of our measurements, we derived a scaling law to correlate  $N$  and  $p_0$ . Figure 4 shows a logarithmic plot of  $N$  versus  $p_0$  for  $T_0 = 140$  K. Regression analysis showed that  $N$  correlates with  $p_0$  according to

$$N = K p_0^{1.8} \quad (5)$$

where  $K$  is a proportionality constant.

We also used the Hagena condensation parameter  $\Gamma^*$ <sup>3,6</sup> to compare our results with those of others. Since Hagena has discussed this parameter at length,<sup>3,6</sup> it will be briefly introduced here. This parameter accounts for both bimolecular and unimolecular reactions governing cluster growth and decay. It is dimensionless and for Ar clusters has the following numerical form:

$$\Gamma^* = 1275(p_0/\text{atm})(d/\text{mm})^{0.85}(T_0/300 \text{ K})^{-2.29} \quad (6)$$

Values of  $\Gamma^*$  were computed using eq 6 for every single set of stagnation conditions used to measure mean cluster sizes. Figure 5 shows a plot of mean cluster sizes  $N$  versus the condensation parameter  $\Gamma^*$ . We used  $\Gamma^*$  as a scaling parameter, because it is universal, even though we are only reporting Ar data. Data from this work are displayed as filled disks. The open symbols pertain to previously published works. A regression including all data but that of Farges et al.<sup>7</sup> (see Discussion section) yielded the following relationship between  $N$  and  $\Gamma^*$ :

$$N = 3.3 \times 10^{-5} \Gamma^{*2.0 \pm 0.1} \quad (7)$$

Note that if only data from this work were used, the exponent of  $\Gamma^*$  would be less.

## Discussion

**Scaling of  $N$  with  $p_0$ .** The exponent we obtained for the variation of cluster size with pressure (eq 5) fits well within

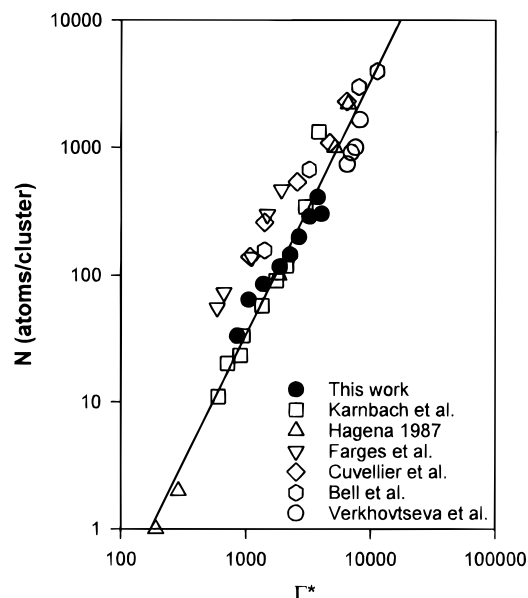


**Figure 5.** Comparison between the mean cluster sizes obtained from this work and some of those previously published. The line is a fit of all data but that of Farges et al.,<sup>7</sup> since it is consistently offset from all other measurements. The data of Verkhovtseva et al.<sup>8</sup> were corrected for the use of a conical nozzle.<sup>3,5</sup>

**TABLE 1: List of the Pressure Scaling Laws for Cluster Sizes from this Work and Previously Published Data**

ref	$q^a$	$d/\text{mm}$	$T_0/\text{K}$	measurement type
2	1.8 <sup>b</sup>	0.49	223–398	time of flight mass spectrometry
3	2.35 <sup>c</sup>			corrected mass spectrometric measurements
15	1.67 <sup>d</sup>			dimer rate of formation
7	1.9	0.2	300	electron diffraction
8	1.8 <sup>e</sup>	0.34	150–500	electron diffraction
9	1.5	0.2	300	scattering + electron diffraction
9	1.35	0.2	300	collisional scattering
this work	1.8	0.17	140	water capture

<sup>a</sup> We use the form  $N \propto p_0^q$ . All sonic nozzles unless indicated. <sup>b</sup>  $N/Z$ , uncorrected for fragmentation, or multiple ionization. <sup>c</sup> Corrected  $N$ , from compiled data. <sup>d</sup> Theoretical. <sup>e</sup> Conical nozzle. These authors reported the dependence  $R_c \propto p_0^{0.6}$ . The number in our table corresponds to  $3 \times 0.6$ .

the range of the reported values for Ar clusters (see Table 1). The result of Farges et al.<sup>7</sup> is of particular significance, since it corresponds to a range of cluster sizes very similar to ours. They also used a sonic nozzle of similar diameter; however, they operated their source at  $T_0 = 300$  K. The agreement between their exponent and ours is very good.

The result reported by Verkhovtseva et al.<sup>8</sup> is in good agreement with ours. This should be regarded with caution since they used a conical nozzle. Such nozzles usually yield somewhat different scaling laws.<sup>2</sup>

Hagena and Obert<sup>2</sup> used a 0.49 mm diameter sonic nozzle with  $T_0$  in the range 223–398 K. They found a  $1.8 \pm 0.1$  exponent for the variation of  $N/Z$  with  $p_0$ , where  $Z$  is the charge of the cluster. These clusters sizes were not corrected for fragmentation or multiple ionization. Applying a correction will increase the exponent. In ref 3 (eq 12), Hagena gave an exponent of 2.35 without error limits, obtained from the fitting of data from different research groups.

Cuvellier et al.<sup>9</sup> plotted both Farges et al.<sup>7</sup> and their own Ar cluster size measurements versus pressure in Figure 4 of ref 9. Both sets of data were obtained for  $d = 0.2$  mm and  $T_0 = 300$  K. By fitting this data, we found that  $N$  depended on  $p_0^{1.5}$ . However, when including only scattering data, we found a  $p_0^{1.35}$

dependence. The reason for this discrepancy remains unclear. Nevertheless, we feel confident that the general agreement between previously reported data and ours validates our method.

**Scaling of  $N$  with  $\Gamma^*$ .** From Figure 5 it is obvious that our results match well with those derived from corrected time-of-flight spectroscopy,<sup>5,6</sup> Rayleigh scattering,<sup>10</sup> and electron diffraction.<sup>8</sup> However, the electron diffraction results of Farges et al.<sup>7</sup> show consistently higher cluster sizes than other measurements. This cannot be attributed to the method they used alone, since the results from ref 8 are in line with all the other measurements. It should also be noted that the determination of diameters from electron diffraction data is not a direct process. Diffraction patterns have to be generated and compared to experimental ones. The typical radius error quoted is  $\pm 20\%$ , which corresponds to a factor of 2 in cluster size. Therefore, different electron diffraction investigators may end up with significantly different cluster sizes for a same set of stagnation conditions. Also, it is possible that the expansion conditions used in Farges et al.'s measurements were significantly different from that of others. The actual geometry of the expansion, i.e., position, size, and geometrical design of the skimmer, as well as the discharge chamber pressure is critical to the cooling of the beam and to cluster formation.<sup>13</sup>

The "slow down" measurements of Cuvellier et al.<sup>9</sup> are in agreement with those of Farges et al.<sup>7</sup> for small clusters but converge with those of others for larger clusters. A similar trend is observed for the results of Bell et al.<sup>10</sup> The reason for this behavior remains unclear.

The overall agreement of the various methods of cluster size measurements is very satisfactory. Therefore, fitting all of the data from Figure 5, except that of Farges et al.,<sup>7</sup> seemed reasonable. We found that  $N$  scaled with  $\Gamma^{*2.0\pm 0.1}$  (eq 7) whereas in eq 12 of ref 3,  $N$  scaled with  $\Gamma^{*2.35}$ . The result from reference 3 was derived using corrected mass spectroscopic data only, whereas that from this work included other methods. This difference might be responsible for this slight discrepancy.

From eq 7 it follows that  $N$  scales with  $p_0^2 T_0^{-4.58}$ . This yields a pressure power exponent of 2, close to that of eq 5. Knuth<sup>15</sup> found that the Ar dimer formation rate scaled with  $T_0^{-4}$ . Since dimer formation is considered to be the first step toward the formation of clusters, one would expect the temperature exponent for cluster sizes to be similar. Indeed, the result from our fit is close to 4.

Verkhovtseva et al.<sup>8</sup> reported the dependence of Ar cluster radii on temperature (see Figure 3 of this reference). They found that  $R_c$  scaled with  $T_0^{-1.4}$ , thus,  $N$  scaled with  $T_0^{-4.2}$ , which compares well with the exponent obtained including other measurements.

Since both  $\Gamma^*$  and  $p_0$  provide a good correlation between our measurements and those previously published, we believe that water capture is a valid and reliable method for the measurement of mean cluster sizes, at least in the range of conditions that we investigated.

Even though  $\Gamma^*$  offers a good correlation between different types of measurements, it is certainly not perfect. This parameter alone does not account for all the aerodynamics that occurs in the expansion region. We believe that the actual design of the cluster source and how it is operated matters a great deal, especially for Campargue type sources where the skimmer performs a real aerodynamic function.<sup>13</sup> Since those

details are generally not reported in the literature, we have to rely on  $\Gamma^*$  to compare cluster sizes.

Some researchers have relied for years on cluster size calibrations based on  $\Gamma^*$  alone to determine their mean cluster sizes. We think that there is no need for this any longer, since most laboratories equipped for cluster production possess the hardware and expertise to perform water capture cluster size measurements. The mean cluster sizes thus obtained should be more accurate, as they would be specific to the actual source design and operation.

Water capture can be readily used outside the range of our conditions. The range we chose was such as to provide us a good overlap with published data. However, one needs to be cautious when considering fairly small clusters ( $N < 30$ ). For small clusters, some of our assumptions can be problematic: the sticking coefficient of water on Ar clusters may not be 1, and the spherical approximation may be too idealistic for accurate results.

Water capture size measurements are not limited to rare gas clusters. This method can be used for molecular van der Waals clusters, which also readily fragment upon electron impact ionization.

## Conclusion

Water capture appears to be a simple, direct, reliable, and inexpensive way of measuring van der Waals cluster mean sizes. It does not require sophisticated scientific apparatus, such as that needed for electron diffraction measurements or Rayleigh scattering. The data analysis is simple, unlike that needed for corrected cluster sizes derived from time-of-flight mass spectrometry or for sizes extracted from collisional scattering experiments.

**Acknowledgment.** We thank Dr. C. R. Brazier for his help in setting up the experimental hardware and for technical discussions and Dr. L. S. Perkins for helpful discussions of cluster doping dynamics.

## References and Notes

- (1) Becker, E. W.; Bier, K.; Henkes, W. *Z. Phys.* **1956**, *146*, 333.
- (2) Hagen, O. F.; Obert, W. *J. Chem. Phys.* **1972**, *56*, 1793.
- (3) Hagen, O. F. *Rev. Sci. Instrum.* **1992**, *63*, 2374.
- (4) Henkes, W. Z. *Naturforsch.* **1961**, *16A*, 842; **1962**, *17A*, 786.
- (5) Karnbach, R.; Joppien, M.; Stapelfeldt, J.; Wörmer, J.; and Möller, T. *Rev. Sci. Instrum.* **1993**, *64*, 2838.
- (6) Hagen, O. F. *Z. Phys. D: At., Mol. Clusters* **1987**, *4*, 292.
- (7) Farges, J.; de Feraudy, M. F.; Raoult, B.; Torchet, G. *J. Chem. Phys.* **1986**, *84*, 3491.
- (8) Verkhovtseva, E. T.; Bondarenko, E. A.; Yaremchenko, V. I.; Doronin, Yu. S. *Chem. Phys. Lett.* **1983**, *97*, 483.
- (9) Cuvellier, J.; Meynadier, P.; de Pujo, P.; Sublemontier, O.; Visticot, J.-P.; Berlande, J.; Lallement, A.; and Mestdagh, J.-M. *Z. Phys. D: At., Mol., Clusters* **1991**, *21*, 265.
- (10) Bell, A. J.; Mestdagh, J.-M.; Berlande, J.; Biquard, X.; Cuvellier, J.; Lallement, A.; Meynadier, P.; Sublemontier, O.; Visticot, J.-P. *J. Phys. D: Appl. Phys.* **1993**, *26*, 994.
- (11) Gough, T.; Mengel, M.; Rowntree, P.; Scoles, G. *J. Chem. Phys.* **1985**, *83*, 4958.
- (12) Lewerenz, M.; Schilling, B.; Toennies, J. P. *J. Chem. Phys.* **1995**, *102*, 8191.
- (13) Campargue, R. *J. Phys. Chem.* **1984**, *88*, 4466.
- (14) Lang, N. C.; Lilienfeld, H. V.; Kinsey, J. L. *J. Chem. Phys.* **1971**, *55*, 3114.
- (15) Knuth, E. L. *J. Chem. Phys.* **1977**, *66*, 3515.